Government of **Western Australia**
Department of **Mines and Petroleum**

RECORD 2016/19

MAPPING IRON ORE ALTERATION PATTERNS IN BANDED IRON-FORMATION USING HYPERSPECTRAL DATA: DRILLHOLE PK12DD001, MT RICHARDSON, YILGARN CRATON, WESTERN AUSTRALIA

by
P Duuring and C Laukamp

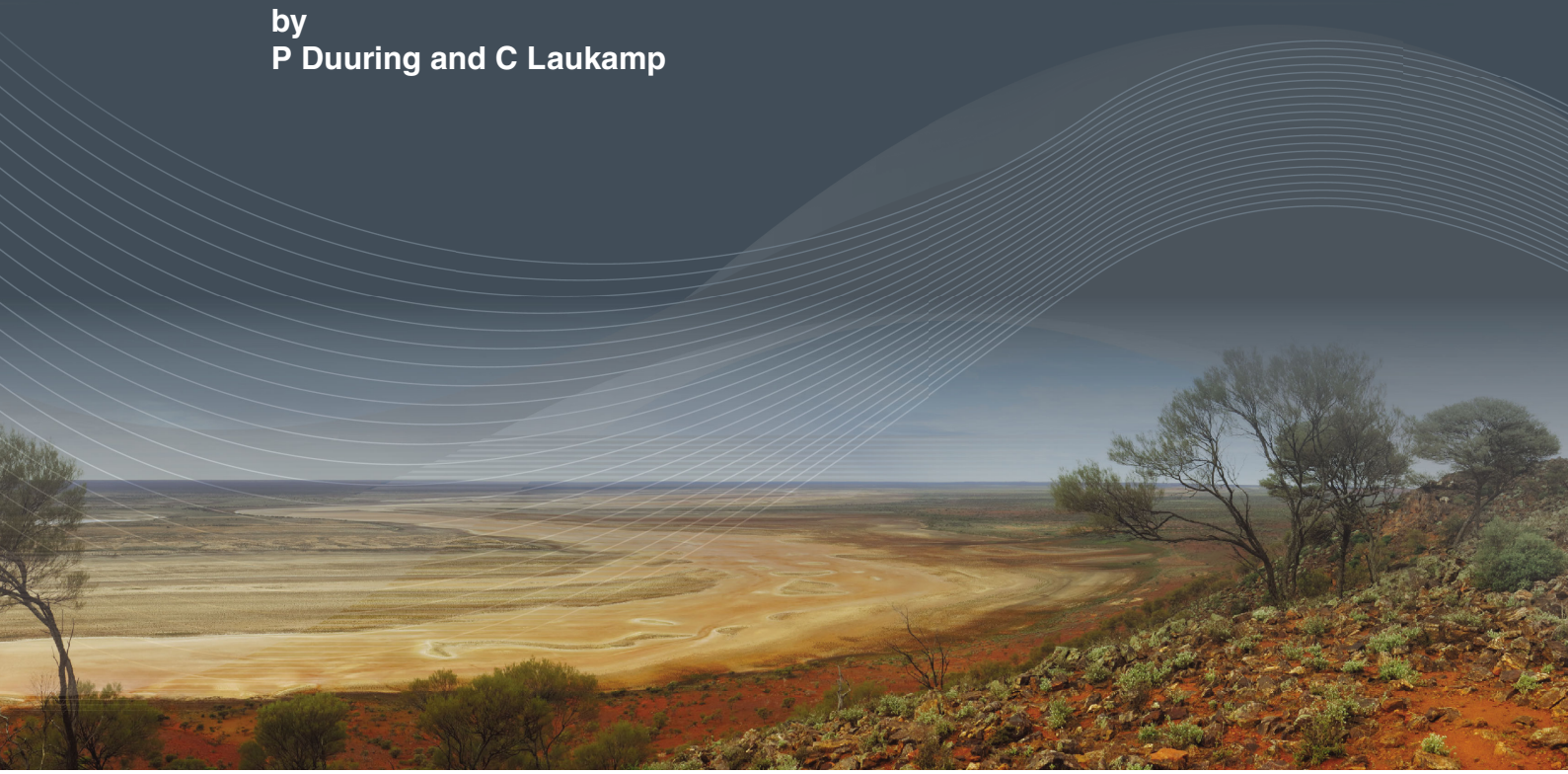

Geological Survey of Western Australia

EXPLORATION INCENTIVE SCHEME

Centre for EXPLORATION TARGETING

CSIRO

Government of **Western Australia**
Department of **Mines and Petroleum**

Record 2016/19

MAPPING IRON ORE ALTERATION PATTERNS IN BANDED IRON-FORMATION USING HYPERSPECTRAL DATA: DRILLHOLE PK12DD001, MT RICHARDSON, YILGARN CRATON, WESTERN AUSTRALIA

by
P Duuring and C Laukamp[1]

1 Western Australian Centre of Excellence for 3D Mineral Mapping, CSIRO Mineral Resources, 26 Dick Perry Avenue, Kensington WA 6151

Perth 2016

Geological Survey of Western Australia

MINISTER FOR MINES AND PETROLEUM
Hon. Sean K L'Estrange MLA

ACTING DIRECTOR GENERAL, DEPARTMENT OF MINES AND PETROLEUM
Tim Griffin

EXECUTIVE DIRECTOR, GEOLOGICAL SURVEY OF WESTERN AUSTRALIA
Rick Rogerson

REFERENCE
The recommended reference for this publication is:
Duuring P and Laukamp C 2016, Mapping iron ore alteration patterns in banded iron-formation using hyperspectral data: drillhole PK12DD001, Mt Richardson, Yilgarn Craton, Western Australia: Geological Survey of Western Australia, Record 2016/19, 19p.

National Library of Australia Card Number and ISBN 978-1-74168-720-0

Grid references in this publication refer to the Geocentric Datum of Australia 1994 (GDA94). Locations mentioned in the text are referenced using Map Grid Australia (MGA) coordinates, Zone 50. All locations are quoted to at least the nearest 100 m.

Published 2016 by Geological Survey of Western Australia
This Record is published in digital format (PDF) and is available online at <www.dmp.wa.gov.au/GSWApublications>.

Further details of geological products and maps produced by the Geological Survey of Western Australia are available from:
Information Centre
Department of Mines and Petroleum
100 Plain Street
EAST PERTH WESTERN AUSTRALIA 6004
Telephone: +61 8 9222 3459 Facsimile: +61 8 9222 3444
www.dmp.wa.gov.au/GSWApublications

Cover image: Elongate salt lake on the Yilgarn Craton — part of the Moore–Monger paleovalley — here viewed from the top of Wownaminya Hill, 20 km southeast of Yalgoo, Murchison Goldfields. Photograph taken by I Zibra for the Geological Survey of Western Australia

Contents

Appendices

Figures

Mapping iron ore alteration patterns in banded iron-formation using hyperspectral data: drillhole PK12DD001, Mt Richardson, Yilgarn Craton, Western Australia

by

P Duuring and C Laukamp[1]

Abstract

Diamond drillhole PK12DD001, located in the Parker area of the Mt Richardson iron prospect, Southern Cross Domain of the Yilgarn Craton, was chosen for hyperspectral analysis based on its intersection of thick intervals of supergene-modified, hypogene iron ore zones that are hosted by banded iron-formation (BIF). Hypogene magnetite ± quartz and specularite ± quartz alteration zones are widely distributed in all BIF macrobands. Supergene alteration is intensely developed in the BIF within 90 m of the present surface. These supergene-altered BIF macrobands are intensely sheared and have a high porosity. Using spectral data, BIF can be distinguished from mafic rocks based on the higher abundance of opaque minerals in BIF, whereas mafic igneous rocks contain more chlorite, amphibole, and kaolinite. Relative to least-altered BIF, hypogene-altered magnetite-rich BIF is identified by higher detectable levels of opaque minerals. No changes were detected in the Fe/Mg ratios for chlorite in hypogene-altered mafic igneous rocks compared with distal areas. Further work is required to evaluate whether some supergene minerals may inherit subtle compositional features from their precursor hypogene alteration minerals. Intensely supergene-altered BIF has a higher detected ferric oxide abundance, goethite/hematite ratio, kaolinite abundance, and lower quartz content, compared with least-altered BIF. Supergene-altered mafic igneous rocks display a decrease or complete absence of amphibole, plagioclase, and pyroxene, as well as metamorphic chlorite and epidote, and hypogene chlorite. These intervals are enriched in kaolinite, goethite (vitreous dominant over ochreous), and hematite.

KEYWORDS: banded iron-formation, hypogene deposits, iron ores, spectral analysis, supergene alteration

Introduction

Reflectance spectral data were collected by the HyLogger-3 for six diamond drillholes from four iron ore deposits located in various greenstone belts throughout the Yilgarn Craton. The sites of interest include the Weld Range (drillhole WRRD0583; Duuring and Laukamp, 2016a), Windarling (drillhole W2DDH007; Duuring and Laukamp, 2016b), Koolyanobbing, and Mt Richardson iron camps (drillholes PK11DD001, PK12DD001 [Duuring and Laukamp, 2016c] and PI12DD002) (Fig. 1). The aim is to identify hypogene and supergene alteration minerals associated with high-grade iron ore (>57 wt% Fe_{total}) in banded iron-formation (BIF) and nearby mafic country rocks.

1 Western Australian Centre of Excellence for 3D Mineral Mapping, CSIRO Mineral Resources, 26 Dick Perry Avenue, Kensington WA 6151

The PK12DD001 diamond drillhole, located in the Parker area of the Mt Richardson prospect, Southern Cross Domain of the Yilgarn Craton (Fig. 1), was scanned using the HyLogger-3 to detect hypogene alteration haloes associated with BIF-hosted iron ore. Of particular interest is whether any textural or mineralogical indicators of hypogene alteration survive the effects of supergene alteration.

Geological overview of the Mt Richardson prospect

The geology of the Mt Richardson prospect has been documented in an unpublished study by Duuring and Hagemann (2013); a summary of that work is given here. The Mt Richardson BIF-hosted iron ore prospect is located in the Southern Cross Domain of the Yilgarn Craton, approximately 530 km northeast of Perth (Fig. 1).

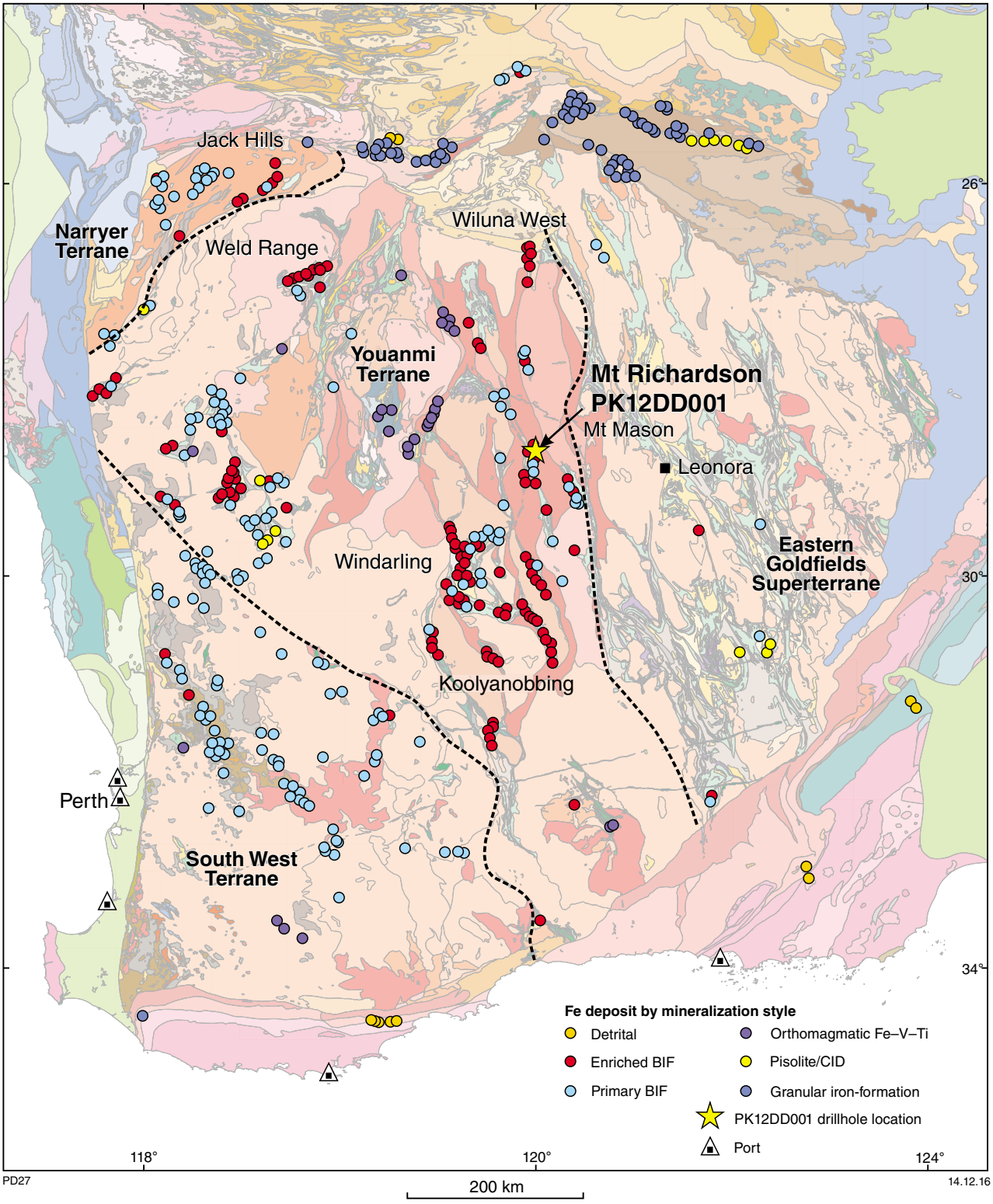

Figure 1. **Distribution of iron ore occurrences in the Yilgarn Craton and location of diamond drillhole PK12DD001 in the Mt Richardson district. Regional geological map from GSWA (2016); iron ore deposits from the GSWA MINEDEX database <www.dmp.wa.gov.au/minedex>. CID – channel iron deposit**

The prospect contains at least 11 BIF macrobands that are 5–90 m thick, steeply west-dipping, and extend along a north-northwest to south-southeast strike. Mafic igneous rocks separate the individual BIF bands (Fig. 2). Goethite–hematite-rich, high-grade ore zones are locally hosted by all exposed BIF bands in the prospect, although the western bands host iron ore zones that are more laterally continuous (Fig. 2).

All rocks in the Mt Richardson prospect are metamorphosed to upper-greenschist facies; the prefix 'meta' applies to all rocks mentioned hereafter but has been omitted from rock descriptions for brevity. Primary stratigraphic relationships in the Mt Richardson prospect area are complicated by complex folding and faulting. Macroscopic fold hinges defined by BIF are preferentially exposed along ridges within the range, with narrower fold limbs commonly faulted and truncated.

BIF macrobands comprise alternating mesobands (1–30 mm thick) of primary iron oxides and quartz. Iron oxide bands commonly represent up to 40 vol% of least-altered BIF, although BIF may grade into banded chert along strike away from the Mt Richardson prospect. Fresh examples of mafic igneous rocks intersected by drillholes include komatiitic basalt, high-Mg tholeiitic basalt, and high-Fe tholeiitic basalt. Texturally, these rocks vary from basalt to dolerite and gabbro. Least-altered, high-Fe tholeiitic basalt comprises primary igneous plagioclase, primary and metamorphic amphiboles, and metamorphic and hydrothermal chlorite and epidote. The margins of most BIF macrobands are intensely weathered and deformed, preventing definitive interpretation of these igneous units as extrusive flows, intrusive units, or a combination of both. A 1–10 m thick blanket of transported sediment covers weathered mafic rocks and BIF along the flanks of most ridges in the Mt Richardson prospect. The detrital unit is poorly sorted and contains subrounded to angular fragments of BIF and mafic igneous rocks cemented by fine-grained goethite.

Bedding in the Mt Richardson prospect strikes north to north-northwest and mainly dips 60–90º west to west-southwest. Four generations of folds are preserved in BIF. The earliest generation of folds is only rarely persevered in outcrop as centimetre-scale, isoclinal F_1 folds that are refolded by the more commonly expressed upright and tight F_2 folds. The limbs of F_2 folds are deformed by 0.1 – 1 m wide, south-striking, steeply west-dipping, ductile shear zones and mylonite zones in BIF. The shear zones and mylonite zones are oriented subparallel to BIF macrobands and contacts with mafic igneous rocks. The timing of the shear zones in the mafic igneous rocks is uncertain, but it is likely there were several discrete episodes of deformation, demonstrated by the local granulation of early quartz veins within the shear zones.

All examples of BIF collected from drillcore and from the surface are at least slightly weathered, as demonstrated by the common pseudomorphic replacement of primary magnetite by hematite (martitization) and the local replacement of these iron oxide minerals by supergene goethite. Least-weathered examples of BIF are best exposed in the easternmost BIF macrobands. In western areas, least-altered BIF is preserved in the centre of thick BIF macrobands, away from the more deformed margins of the BIF. Least-altered BIF mainly comprises 35–40 wt% Fe_{total}, 38–50 wt% SiO_2, 0.02 – 2.00 wt% Al_2O_3, 0.020 – 0.079 wt% P_2O_5, 0.005 – 0.030 wt% MgO, and 5–10 wt% loss on ignition (LOI) content.

Hypogene magnetite–talc alteration is present as veins and wallrock alteration associated with <2 m thick, ductile shear zones in BIF. These shear zones are primarily located along both margins of BIF macrobands. The disseminated magnetite and talc define wallrock alteration zones in BIF that extend up to 25 m away from these sheared margins. Hypogene magnetite–talc alteration zones are not enriched in Fe_{total} relative to least-altered BIF, but these zones have lower competency and enhanced permeability. Fresh and intensely magnetite–talc-altered BIF comprises 32–46 wt% Fe_{total}, 36–38 wt% SiO_2, 0.14 – 6.00 wt% Al_2O_3, 0.010 – 0.230 wt% P_2O_5, and 0.01 – 0.18 wt% MgO. Later hypogene specularite alteration of BIF is widest and most intensely developed within the most westerly BIF macrobands in the Mt Richardson prospect. At the prospect scale, hypogene specularite alteration intensity in the BIF macrobands increases with strain and shearing intensities from east to west. BIF bands and earlier hypogene alteration zones are locally cut by several generations of 1–50 cm thick quartz ± carbonate ± pyrite veins.

Supergene alteration zones are located near surface and extend to greater depths along the deformed margins of BIF macrobands. In these areas, primary iron oxide bands and hypogene magnetite in BIF are oxidized to martite, whereas primary quartz bands are leached, or replaced by supergene goethite. The resulting supergene-altered BIF is iron rich and silica poor, with high porosity. Primary banding and secondary schistosity in BIF are destroyed by supergene alteration, resulting in a massive to fragmental-textured rock. Supergene-altered BIF comprises 58–69 wt% Fe_{total}, 0.5 – 6.0 wt% SiO_2, 0.16 – 5.00 wt% Al_2O_3, 0.010 – 0.090 wt% P_2O_5, and 0.02 – 0.06 wt% MgO.

Least-altered mafic rocks are massive and homogeneous. The rocks comprise mostly primary amphibole and plagioclase, with metamorphic chlorite and epidote. Hypogene alteration zones in mafic igneous rocks are proximal to mineralized BIF macrobands and are characterized by an increase in hypogene chlorite and a decrease in primary amphibole and plagioclase. Supergene alteration is intensely developed along the contacts of BIF, overprinting and obscuring hypogene alteration zonation patterns. In more distal areas, quartz–magnetite–pyrite shear veins cut basalt, and are in turn cut by quartz–carbonate veins.

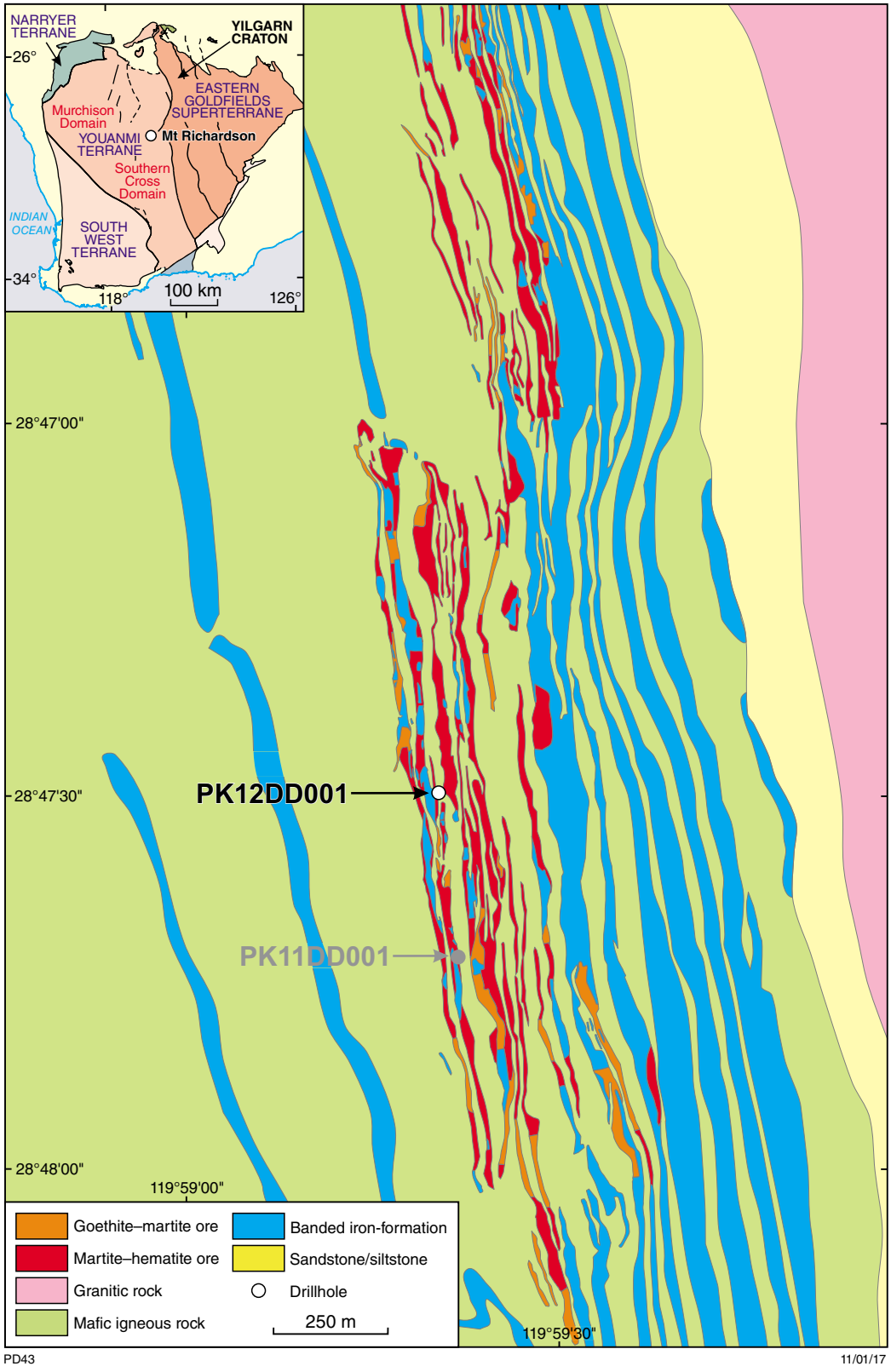

Figure 2. Solid geology of the Mt Richardson prospect, showing the distribution of rock types, ore zones, and the location of drillhole PK12DD001

Results from the conventional logging of diamond drillhole PK12DD001

The PK12DD001 drillhole was drilled from the surface (MGA 791779E 6811437N) at an angle of 36° towards 082° for a total length of 172.5 m. The PK12DD001 drillhole was chosen based on its intersection of several banded iron-formation (BIF) macrobands, hypogene iron ore zones in BIF and surrounding mafic igneous rocks, with local effects of supergene alteration. The drillhole intersects a 22 m thick, BIF macroband and several 1–7 m thick BIF macrobands that are separated by 1–77 m thick intervals of massive, fine-grained mafic rocks or dolerite (Fig. 3). A four metre thick, transported, poorly consolidated sediment unconformably overlies mafic rocks at the top of the hole. Supergene alteration intensity decreases with depth, but is more intense along the deformed margins of BIF. All BIF macrobands, apart from the lowermost BIF5 macroband, host thick intervals of high-grade iron ore (>57 wt% Fe_{total}). The BIF and fine-grained mafic rocks are intensely schistose over the interval containing the high-grade iron ore zones, from 35 to 100 m depth.

Rock types

All BIF macrobands (BIF1 to BIF5; Fig. 3) are intensely replaced by hypogene and supergene minerals, with only minor least-altered BIF preserved in discrete intervals of the BIF5 macroband, from about 165–170 m. The least-altered BIF is grey, thickly banded (1 cm thick bands), with alternating bands of quartz and magnetite–martite. The rock comprises mainly Fe_{total} (40–50 wt%) and SiO_2 (26–40 wt%), with minor LOI content (1.24 – 2.24 wt%), Al_2O_3 (0.24 – 0.31 wt%), and P_2O_5 (0.020 – 0.050 wt%).

Rare, least-altered, fine-grained mafic rocks are located within the Mafic6 interval, from about 130 to 131 m. This rock is green, schistose, and chlorite rich, with a weak supergene goethite overprint. Geochemical data are not available for least-altered Mafic6; instead, most geochemical data are provided for supergene-altered, mafic igneous rocks located within about 10 m of BIF margins. A comparison of least-mobile element ratios (e.g. Al_2O_3 vs TiO_2) for fine-grained mafic rocks demonstrates at least two main compositional groups. The first compositional group includes rocks from the Mafic1, Mafic2, Mafic4, Mafic7, and part of the Mafic5 intervals. The second group includes Mafic3 and part of the Mafic5 intervals (Fig. 4). Linear trends defined by Al_2O_3 vs TiO_2 ratios are likely the product of supergene alteration, and potentially also primary magmatic fractionation trends recorded during the crystallization of these rocks (Fig. 4). The intense supergene alteration along primary contacts prevents genetic interpretation of these mafic igneous rocks, whether they formed as a series of extrusive flows, as intrusions, or a combination of both styles.

Hypogene alteration of BIF

Least-weathered examples of hypogene-altered BIF are present in the BIF3 macroband from 65.5 to 71.5 m (Fig. 3). In this interval, BIF is dark grey to black, thinly banded, and displays a moderate to intense schistose fabric. In some areas, <1 mm diameter crystals of hypogene specularite dominate, resulting in a more massive secondary texture in BIF. Magnetite in primary iron oxide-rich bands is replaced by martite. Unlike the PK11DD001 drillhole, where early hypogene magnetite–quartz alteration zones are preserved in BIF (Duuring and Laukamp, 2016c), the intense supergene alteration expressed in the PK12DD001 drillhole has mostly destroyed the mineralogical and textural evidence for early magnetite–quartz alteration. Compared with the least-altered BIF5 interval, the least-weathered hypogene specularite-altered zones in BIF3 from 65.5 to 71.5 m display higher Fe_{total} (68.26 – 68.91 wt%) and Al_2O_3 (0.40 – 0.71 wt%), and lower values for SiO_2 (0.59 – 0.90 wt%), P_2O_5 (0.009 – 0.016 wt%), and LOI content (0.29 – 0.38 wt%). The major enrichment in Fe_{total} and depletion in SiO_2 in the hypogene-altered BIF is due to the addition of hypogene hematite with negligible hypogene quartz.

Hypogene alteration of mafic igneous rocks

Fresh, hypogene-altered, fine-grained mafic rocks were not recognized in drillhole PK12DD001 due to the widespread replacement of primary and hypogene minerals by intense supergene alteration. Fresh fine-grained mafic rocks without hypogene alteration are only preserved in Mafic6 about 40 m below the contact of BIF4, from 129 to 130 m.

Supergene alteration of BIF

The BIF1, BIF2, and BIF4 macrobands are schistose and intensely altered to hypogene specularite. These intervals are additionally affected by strong, supergene, goethite-martite alteration, demonstrated by the widespread replacement of primary quartz-rich bands by goethite and the oxidation of magnetite-rich bands to martite. These rocks are dark grey to brown, soft and friable, schistose, have about 10% porosity, and contain abundant, fine-grained, crystalline hematite. Primary banding is poorly preserved and is overprinted by the strong schistosity defined by aligned crystalline hematite. Ochreous goethite is absent in BIF. Compared with the least-altered BIF5 interval, the intensely supergene-altered BIF2 from 38 to 56 m displays higher Fe_{total} (49.25 – 66.76 wt%) and Al_2O_3 (0.13 – 4.69 wt%), comparable P_2O_5 (0.015 – 0.068 wt%) and LOI contents (0.81 – 5.86 wt%), and lower values for SiO_2 (1.51 – 27.38 wt%). The major enrichment in Fe_{total} and depletion in SiO_2 in the supergene-altered BIF relative to least-altered BIF is explained by the addition of supergene goethite–hematite and removal of quartz.

Compared with hypogene specularite-altered BIF, the higher abundance of goethite in supergene-altered BIF corresponds with an increase in LOI content (i.e. from 0.32 to 1.83 wt%), but a decrease in Fe_{total} content (i.e. from 68 to 63 wt% Fe_{total}).

Supergene alteration of mafic igneous rocks

Basalt located within 100 m of the surface and within 10 m of the upper contact of BIF5 (from 155 to 165 m) is intensely supergene altered. These intervals are mostly red-brown, fine grained, locally schistose, and comprise vitreous goethite, cryptocrystalline hematite, and kaolinite. Ochreous goethite is locally intense, but limited to within 5 m of intensely sheared margins of BIF macrobands. In fine-grained mafic rocks, primary igneous amphibole, pyroxene, olivine, and plagioclase, and metamorphic epidote and chlorite, are replaced by supergene hematite, goethite, and kaolinite.

Supergene-altered, fine-grained mafic rocks proximal to BIF-hosted hypogene iron ore zones (from 33 to 36 m) comprise mostly SiO_2 (36.00 – 43.23 wt%), Al_2O_3 (24.37 – 27.79 wt%), Fe_{total} (15.79 – 17.00 wt%), and LOI contents (9.21 – 10.77 wt%), with minor TiO_2 (0.39 – 0.52 wt%), P_2O_5 (0.005 – 0.020 wt%), MgO (0.02 – 0.030 wt%), MnO (0.005 – 0.010 wt%), and CaO (0.005 – 0.010 wt%). With proximity to the upper margin of BIF2, the fine-grained mafic rocks are enriched in Fe_{total}, P_2O_5, LOI, Al_2O_3, and TiO_2, but depleted in SiO_2.

Results of hyperspectral data acquisition and processing

Method

A detailed description of the general principles of the HyLogger-3 is provided by Hancock et al. (2013) and Duuring and Laukamp (2016a). The HyLogger-3 hyperspectral scanning system developed by CSIRO in Australia uses reflectance spectra of scanned diamond drillcore to identify mineral abundances and mineral chemistry (Hunt, 1977; Clark and Roush, 1984). The HyLogger-3 operated by GSWA in Perth detects radiation reflected from the drillcore within the visible to near infrared (VNIR, 380–1000 nm), short wave infrared (SWIR, 1000–2500 nm) and thermal infrared (TIR, 6000–14000 nm) parts of the electromagnetic spectrum. The HyLogger-3 uses an automated x–y table that moves the core tray at intervals of 1 cm data resolution (Haest et al., 2012a). The reflectance spectra are cross-calibrated using a Spectralon panel. During the nondestructive scanning process, the HyLogger-3 also captures high-resolution digital core images, which are referenced to a standard set of Munsell colours. The hyperspectral data are then processed to determine the abundance of minerals, as well as their composition and/or crystallinity, based on the wavelength, depth and width of diagnostic absorption features. Algorithms applied in this project were developed by CSIRO (Laukamp, 2011; Haest et al., 2012a; Sonntag et al., 2012) and were used in this study to determine mineral abundance and composition of iron oxides, including hematite, vitreous goethite and ochreous goethite, and other minerals such as chlorites, carbonates, amphiboles, white micas, and kaolin group minerals (Appendix 6).

The collected VNIR, SWIR, and TIR spectral signatures were processed using the commercial software 'The Spectral Geologist' (TSG). Mineral abundance and composition information are extracted using the multiple feature extraction method (Cudahy et al., 2008; Laukamp et al., 2010). Positions and depths of absorption features in this study were calculated by locally removing the hull from the reflectance spectra to reduce the influence of instrument or atmospheric noise (Cudahy et al., 2008).

Reflectance spectral geoscience products that are potentially useful for the study of BIF-hosted iron ore include: 1) opaque minerals (e.g. magnetite and pyrite); 2) ferric oxide minerals (e.g. hematite and goethite); 3) kaolinite composition (e.g. crystalline vs poorly crystalline); 4) white micas (e.g. muscovite and phengite); 5) ferrous iron and magnesium-bearing sheet silicates (e.g. actinolite and chlorite); 6) carbonate minerals (e.g. calcite, dolomite, and magnesite; Duuring and Laukamp, 2016a). In all provided examples of reflectance spectral data products, the relative abundance of minerals is indicated by the distribution of the data with vertical depth down the drillhole. The horizontal axes for these plots are without units and show the relative abundance of data. In most plots, the mineral abundance data are coloured on the basis of mineral composition.

Rock types

In the PK12DD001 drillhole, BIF can be accurately distinguished from mafic rocks based on the former's higher abundance of opaque minerals (i.e. primary or hypogene magnetite; Fig. 3). Basalt contains more chlorite, amphibole, and kaolinite than BIF; however, the presence of chlorite and amphibole is greatly affected by supergene alteration, lessening the usefulness of these spectral products for distinguishing protoliths in weathered rocks.

Transported sediment located in the uppermost 4 m of the drillcore contains poorly ordered kaolinite, which has a different spectral signature to more-ordered kaolinite detected at deeper intervals in the hole (Fig. 5).

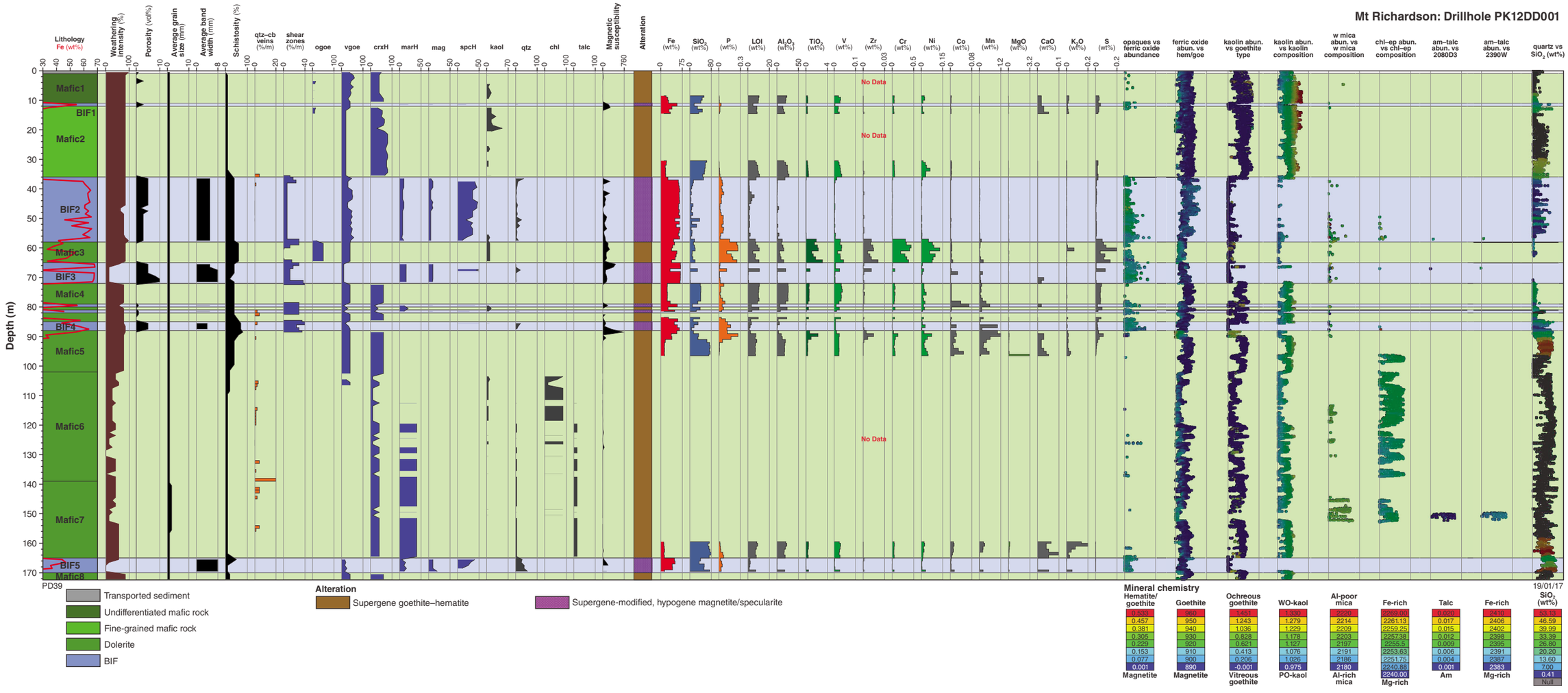

Figure 3. **Hyperspectral log for PK12DD001. Abbreviations: abun – abundance; am – amphibole; cb – carbonate; chl – chlorite; crxH – crystalline hematite; ep – epidote; ferric oxide – ferric oxide minerals; goe – goethite; kaol – kaolinite; LOI – loss on ignition; mag – magnetite; marH – martite; ogoe – ochreous goethite; opaques – opaque minerals; PO-kaol – poorly ordered kaolinite; qtz – quartz; spcH – specular hematite; vgoe – vitreous goethite; w mica – white micas; WO-kaol – well-ordered kaolinite**

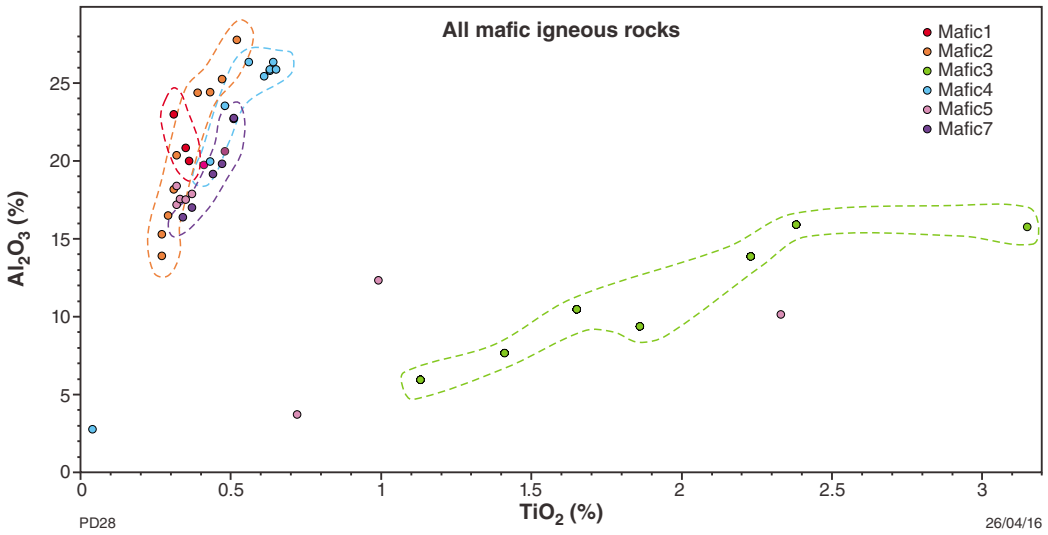

Figure 4. Immobile element ratios Al_2O_3 vs TiO_2 for mafic igneous rocks. Two main compositional groups are demonstrated, both of which display internal fractionation geochemical trends most likely associated with evolution of the magma, combined with the overprinting effects of supergene alteration. Mafic3 and Mafic5 intervals display the greatest difference from other mafic intervals and potentially represent genetically different mafic igneous rocks to the other sampled intervals.

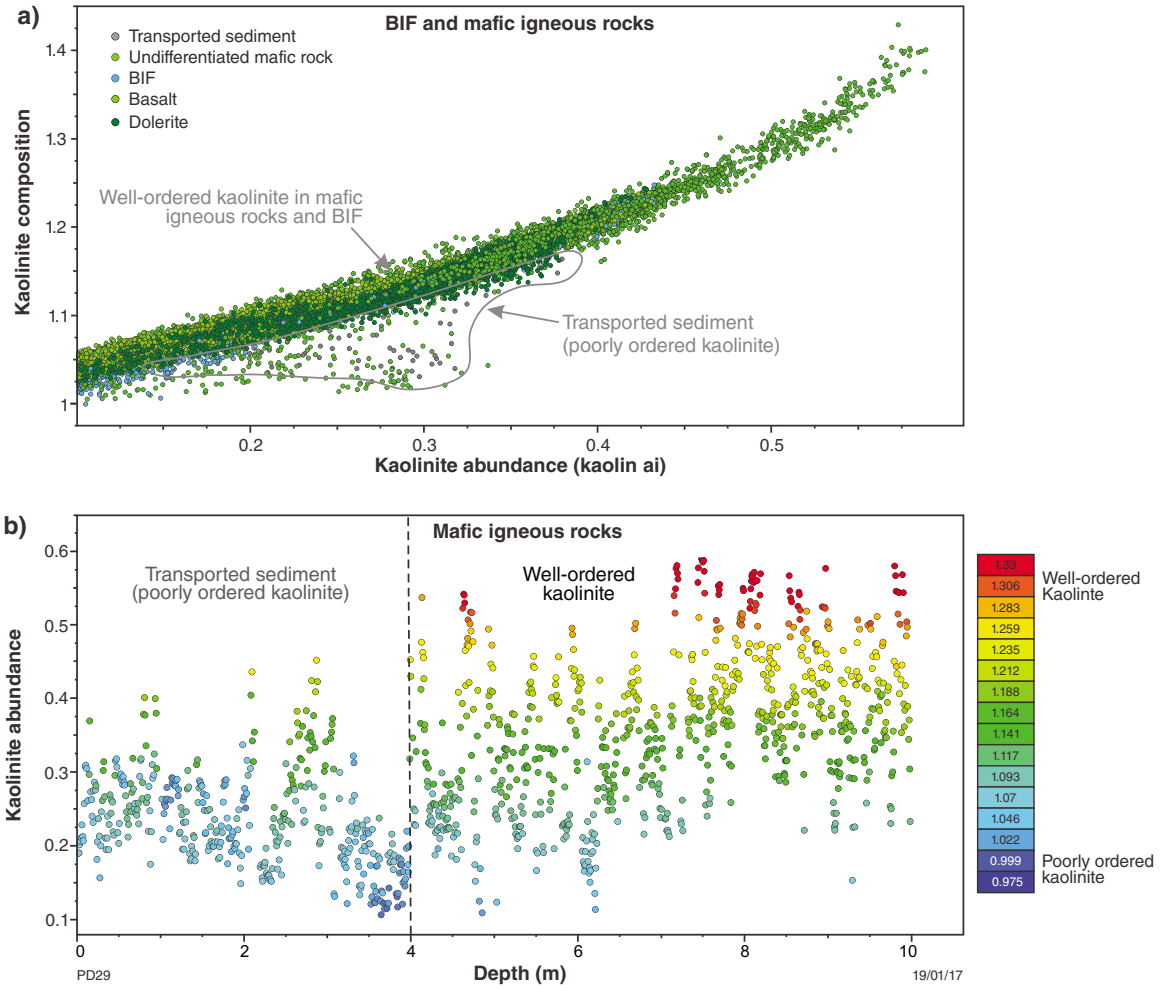

Figure 5. Kaolinite abundance and composition vs rock type: a) transported sediment in the first 4 m of the drillhole displays poorly ordered kaolinite; b) supergene-altered mafic igneous rocks at greater depths contain more crystalline kaolinite

Hypogene alteration of BIF

All BIF macrobands display hypogene alteration. However, the BIF3 macroband is the least-weathered and most intensely altered by the addition of magnetite, with low abundances of quartz, hematite, and goethite, as well as some of the highest Fe_{total} concentrations (Appendix 1a,b and Appendix 2a). The magnetite-rich BIF3 macroband displays a uniformly high magnetic susceptibility (Appendix 1e), low P_2O_5 content (Appendix 2b), high Mn content (Appendix 3a), and locally high S (Appendix 4f), Cu (Appendix 5a), Zn (Appendix 5b), and Pb (Appendix 5c) contents.

Hypogene alteration of mafic igneous rocks

Hypogene alteration zones in mafic igneous rocks cannot be accurately defined in this drillhole due to their replacement by supergene alteration minerals in proximity to BIF-hosted high-grade iron ore. Primary igneous amphibole is only detected in the Mafic7 interval from 150 to 153 m, where it is Mg rich (Fig. 3). In the Mafic5, Mafic6, and Mafic7 intervals, amphibole is mostly replaced by metamorphic or hypogene chlorite (Fig. 3). No systematic change in Fe/Mg ratio for chlorite relative to chlorite abundance was detected over this interval of core (Fig. 6). In this drillhole, the absence of chlorite preserved in supergene-altered, proximal zones to BIF (i.e. within 10 m of contacts) hinders the detection of gradients in hypogene alteration zones in the mafic igneous rocks.

The apparent detection of white mica in two main intervals of fine-grained mafic rocks (i.e. 113–131 m and 144–152 m; Fig. 3) is likely to be a result of the misidentification of white mica by the processing script. Careful inspection of the individual spectra suggests complications associated with the presence of amphibole. Smectite was similarly detected by the smectite abundance script, but was most likely overestimated because of the presence of amphibole.

Supergene alteration of BIF

Supergene alteration is intensely developed in BIF1, BIF2, and BIF4 macrobands, which are located within 90 m of the present surface. BIF3 and BIF5 display weak supergene alteration (Appendix 1b). Compared with the least-altered BIF5 macroband, the intensely supergene-altered BIF2 macroband contains comparable opaque mineral abundances, but higher ferric oxide abundance, higher kaolinite abundance, and lower quartz abundance (Fig. 3 and Appendix 1a). Texturally, the supergene-altered BIF has a higher porosity and more intense schistosity (Appendix 1c,d). Goethite-rich examples of supergene-altered ore contain lower Fe_{total} and higher P_2O_5 contents compared with hypogene magnetite-rich ore zones (Appendix 2a,b). Most other elements (e.g. CaO, K_2O, MnO, Al_2O_3, Cr, Ni, Co, TiO_2, V, Zr, S, Cu, Zn, and Pb) are depleted in the strongly goethite-rich samples relative to least-altered and hypogene-altered BIF (Appendices 1–5).

Supergene alteration of mafic igneous rocks

Intense supergene alteration of mafic rocks within the uppermost 95 m of the drillhole completely destroys primary amphibole, plagioclase, and pyroxene, as well as metamorphic chlorite and epidote, and hypogene chlorite (Fig. 3). The interval comprises mainly crystalline kaolinite, goethite (vitreous dominant over ochreous), and hematite. Interestingly, quartz abundance is high in fine-grained mafic rocks, but is lowest in the intensely supergene-altered zones proximal to BIF-hosted iron ore,

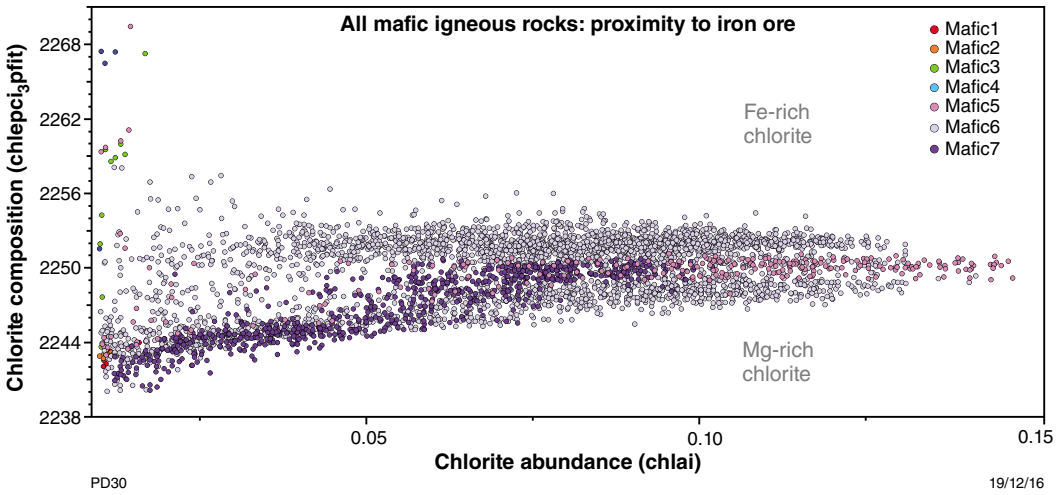

Figure 6. Chlorite abundance and composition in mafic igneous rocks. Chlorite composition becomes more Fe rich with proximity to BIF-hosted iron ore zones as demonstrated by the differences in Fe/Mg ratios for intervals from Mafic5 to Mafic7. However, this relationship is likely complicated by the inheritance of compositional variations from protoliths, as demonstrated by the Fe/Mg ratio of Mafic5.

such as the Mafic3 and Mafic4 intervals (Fig. 3). In some cases, zones of high quartz abundance may be correlated with narrow zones of quartz veins. In other areas, such as in the Mafic2 interval, it is less clear what is causing the high quartz abundance detected in fine-grained mafic rocks.

Conclusions

The PK12DD001 diamond drillhole, located in the Parker area of the Mt Richardson iron prospect, intersects multiple macrobands of BIF, mafic igneous rocks, and BIF-hosted hypogene iron ore. All rock types and hypogene alteration zones are affected by supergene alteration, resulting in significant changes in mineral composition, textures, and whole-rock and trace element geochemistry.

BIF can be accurately distinguished from fine-grained mafic rocks based on its higher abundance of opaque minerals, whereas mafic igneous rocks contain more detected chlorite, amphibole, and kaolinite. However, care must be taken when interpreting lithologies based on the presence of chlorite and amphibole due to the widespread replacement of these minerals during late supergene alteration.

Hypogene alteration zones are poorly preserved in drillhole PK12DD001 due to widespread supergene alteration. Rare preservation of hypogene magnetite-rich BIF is restricted to the BIF3 macroband and is identified by higher detectable levels of opaque minerals and Fe_{total} values, and corresponding low abundances of SiO_2, quartz, and ferric oxide minerals. Hypogene alteration zones in mafic igneous rocks cannot be accurately defined in this drillhole due to their replacement by supergene alteration minerals in proximity to BIF-hosted high-grade iron ore. No changes were detected in the Fe/Mg ratios for chlorite in mafic igneous rocks with proximity to BIF-hosted iron ore zones.

Intensely supergene-altered BIF has a more highly detected ferric oxide abundance, goethite/hematite ratio, kaolinite abundance, and lower quartz content, compared with least-altered BIF. Supergene-altered mafic igneous rocks display a decrease in, or complete absence of, amphibole, plagioclase, and pyroxene, as well as metamorphic chlorite and epidote, and hypogene chlorite. These intervals are enriched in kaolinite, goethite (vitreous dominant over ochreous), and hematite.

Drillhole PK12DD001 demonstrates that a combination of hypogene and supergene alteration was crucial for the enrichment of iron oxide minerals and removal of quartz in BIF to form high-grade iron ore zones. Widespread supergene alteration masks any potential gradients in hypogene alteration mineral abundance or mineral chemistry in mafic igneous rocks proximal to BIF-hosted iron ore.

Acknowledgements

This study was funded by the Geological Survey of Western Australia's Exploration Incentive Scheme (a Royalties for Regions initiative). We thank Cliffs Natural Resources for providing access to drillhole PK12DD001.

References

Bishop, JL, Lane, MD, Dyar, MD and Brown, AJ 2008, Reflectance and emission spectroscopy study of four groups of phyllosilicates: smectites, kaolinite-serpentines, chlorites and micas: Clay Minerals, v. 43, p. 35–54.

Clark, RN and Roush, TL 1984, Reflectance spectroscopy: Quantitative analysis techniques for remote sensing applications: Journal of Geophysical Research: Solid Earth, v. 89, no. B7, p. 6329–6340.

Cudahy, TJ, Jones, M, Thomas, M, Laukamp, C, Caccetta, M, Hewson, RD, Rodger, AR and Verrall, M 2008, Next generation mineral mapping: Queensland airborne HyMap and satellite ASTER surveys 2006–2008: CSIRO, Open File Report P2007/364, 120p.

Duke, E 1994, Near infrared spectra of muscovite, Tschermak substitution, and metamorphic reaction progress: Implications for remote sensing: Geology, v. 22, p. 621–624.

Duuring, P and Hagemann, SG 2013, Controls for iron mineralisation hosted by banded iron-formation in the Mt Richardson district, Yilgarn Craton, Western Australia: The University of Western Australia, Geological Survey of Western Australia (unpublished report), 28p.

Duuring, P and Laukamp, C 2016a, Mapping iron ore alteration patterns in banded iron-formation using hyperspectral data: Beebyn deposit, Yilgarn Craton, Western Australia: Geological Survey of Western Australia, Record 2016/16, 18p.

Duuring, P and Laukamp, C 2016b, Mapping iron ore alteration patterns in banded iron-formation using hyperspectral data: Windarling iron camp, Yilgarn Craton, Western Australia: Geological Survey of Western Australia, Record 2016/17, 14p.

Duuring, P and Laukamp, C 2016c, Mapping iron ore alteration patterns in banded iron-formation using hyperspectral data: drillhole PK11DD001, Mt Richardson, Yilgarn Craton, Western Australia: Geological Survey of Western Australia, Record 2016/18, 15p.

Geological Survey of Western Australia 2016, 1:500 000 State interpreted geology of Western Australia, 2016: Geological Survey of Western Australia, digital data layer, <www.dmp.wa.gov.au/geoview>.

Haest, M, Cudahy, T, Laukamp, C and Gregory, S 2012a, Quantitative mineralogy from infrared spectroscopic data. (I) Validation of mineral abundance and composition scripts at the Rocklea channel iron deposit in Western Australia: Economic Geology, v. 107, no. 2, p. 209–228.

Haest, M, Cudahy, T, Laukamp, C and Gregory, S 2012b, Quantitative mineralogy from visible to shortwave infrared spectroscopic data. (II) Three-dimensional mineralogical characterisation of the Rocklea channel iron deposit, Western Australia: Economic Geology, v. 107, no. 2, p. 229–249.

Hancock, EA, Green, AA, Huntington, JF, Schodlok, MC and Whitbourn, LB 2013, HyLogger-3: Implications of adding thermal-infrared sensing: Geological Survey of Western Australia, Record 2013/3, 24p.

Hunt, G 1977, Spectral signatures of particular minerals in the visible and near infrared: Geophysics, v. 42, no. 3, p. 501–513, doi:10.1190/1.1440721.

Laukamp, C 2011, Short wave infrared functional groups of rock-forming minerals: CSIRO, Report EP115222, 13p.

Laukamp, C, Caccetta, M, Chia, J, Cudahy, T, Gessner, K, Haest, M, Liu, YC, Ong, C and Rodger, A 2010, The uses, abuses and opportunities for hyperspectral technologies and derived geoscience information: AIG Bulletin; Geo-Computing 2010 Conference, Brisbane, September 2010, no. 51, p. 73–76.

Laukamp, C, Termin, KA, Pejcic, B, Haest, M and Cudahy, T 2012, Vibrational spectroscopy of calcic amphiboles — applications for exploration and mining: European Journal of Mineralogy, v. 24, p. 863–878.

Sonntag, I, Laukamp, C and Hagemann, SG 2012, Low potassium hydrothermal alteration in low sulfidation epithermal systems as detected by IRS and XRD: An example from the Co-O mine, Eastern Mindanao, Philippines: Ore Geology Reviews, v. 45, p. 47–60.

Appendices

Appendices 1–5

Ternary plots showing quartz, opaque mineral, and ferric oxide mineral abundances detected by the HyLogger-3 for BIF. Indicated fields for least-altered BIF, hypogene-altered BIF, and supergene-altered BIF apply to each ternary diagram. Data for various rock properties, major element oxide abundances, and trace element abundances plotted within these diagrams show how the measured properties and abundances vary according to the degree of alteration.

Appendix 6

Description of spectral scripts for geoscience products

Appendix 1

Ternary plots for BIF: physical features and SiO_2 content

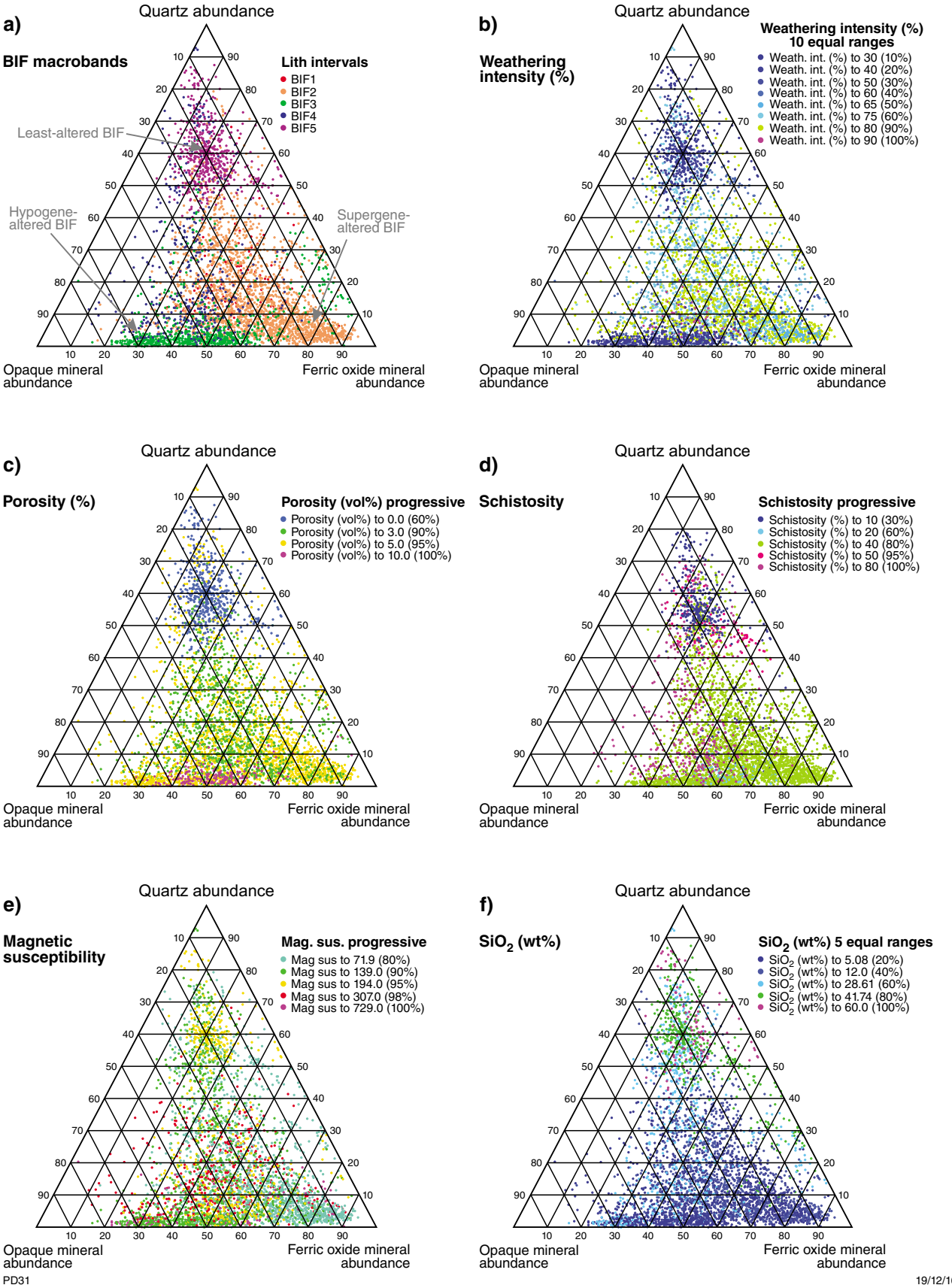

PD31

19/12/16

Appendix 2

Ternary plots for BIF: Fe, P, LOI, CaO, K_2O, MgO

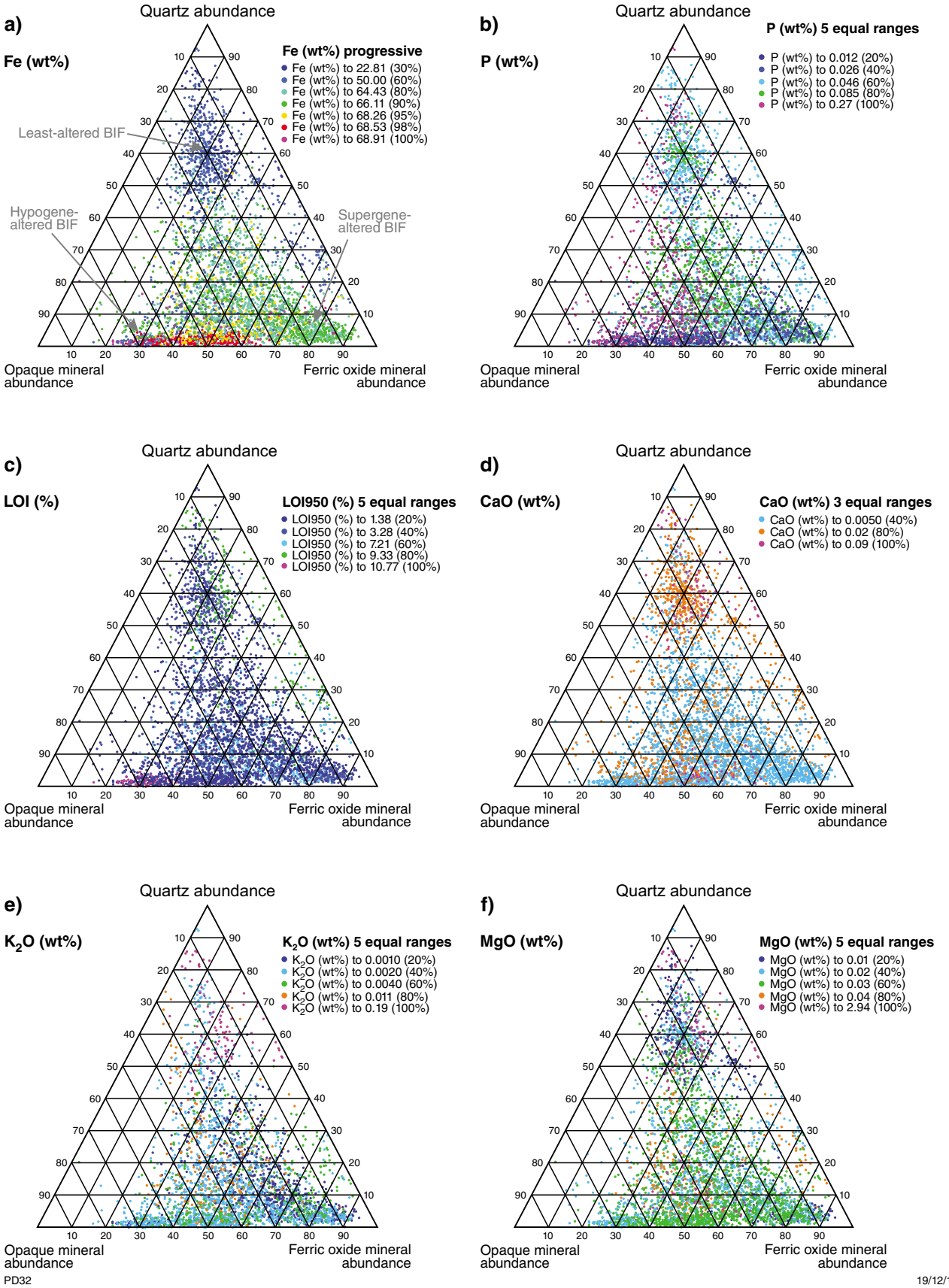

Appendix 3

Ternary plots for BIF: Mn, FMI spectral data, Al_2O_3, kaolinite abundance, Cr, Ni

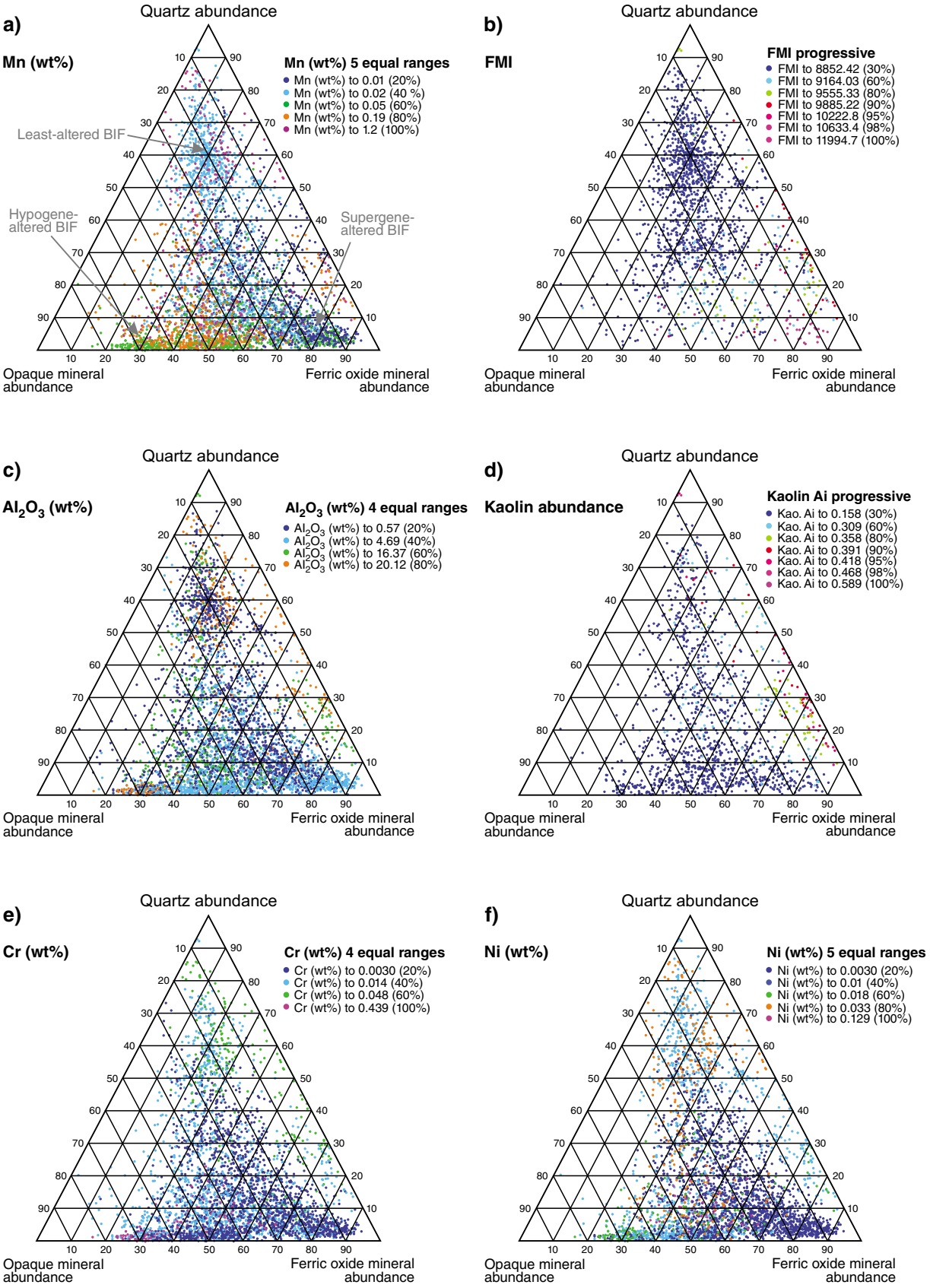

PD33

19/12/16

Appendix 4

Ternary plots for BIF: Co, TiO_2, V, Zr, As, S

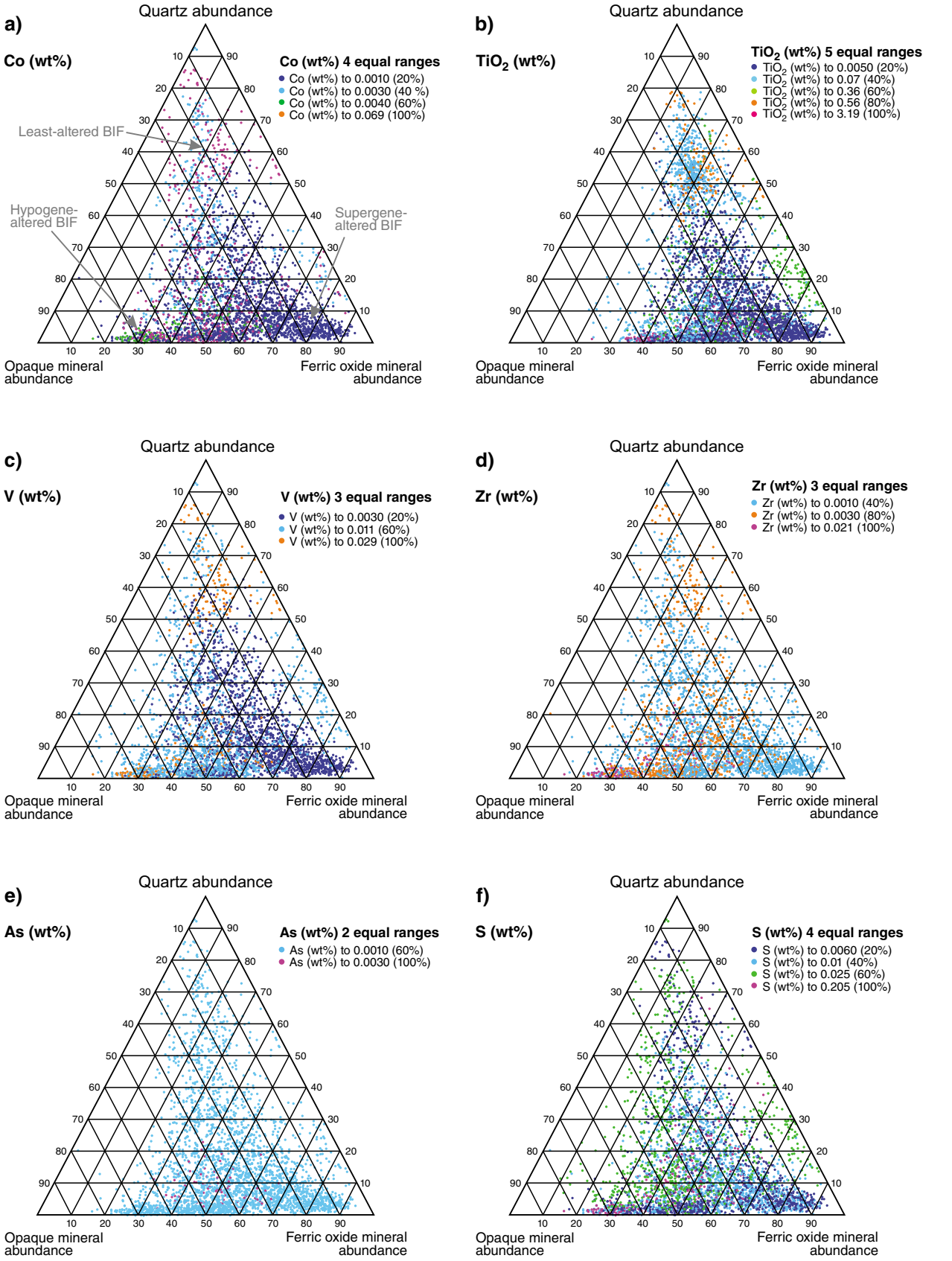

PD34 21/12/16

Appendix 5

Ternary plots for BIF: Cu, Zn, Pb, goethite/hematite ratio

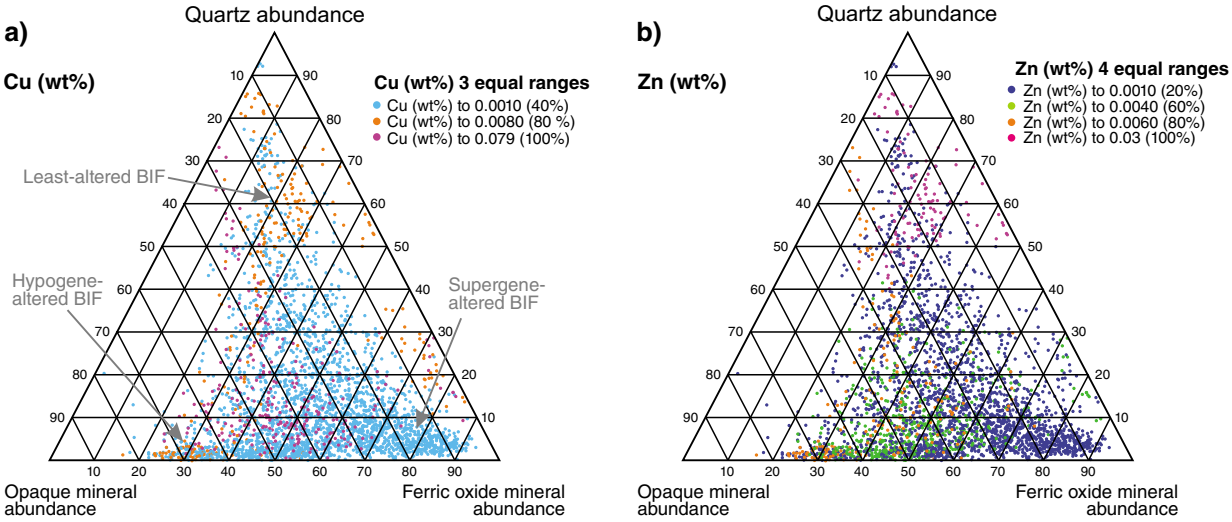

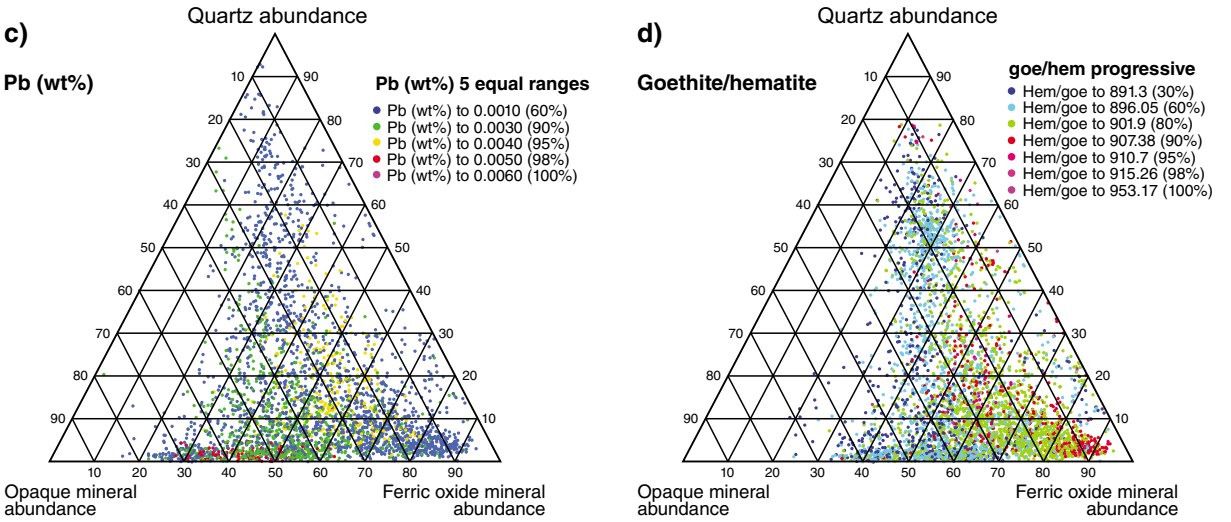

PD35

19/12/16

Appendix 6

Description of spectral scripts for geoscience products

Product name	Minerals detected	Base algorithm	Filters/Masks	Lower stretch limit	Upper stretch limit (based on UGD1683)	Related publication	Comments on general accuracy
Opaques abundance	Sulfides, carbon black (e.g. ash, magnetite, or Mn oxides)	(R456)/(R1650) OPAQUES_450D1650	albedo @ 1650 nm <30%	0.25: low content	Not specified yet – depending on results from other drillcores		Moderate: errors introduced by a lack of Fe^{3+} absorption in the visible, e.g. iron oxide poor clays that, in theory, would be masked by the <30% albedo but may be in partial 'shadow'
Ferric oxide abundance (Ferric_oxide_abundance.txt)	Hematite, goethite, jarosite	Continuum removed depth of the 900 nm absorption calculated using a fitted 2nd order polynomial between 776 and 1050 nm. 900D	R450 > R1650	0.04: low content	Not specified – depending on whole dataset	Further developed on the basis of Haest et al. (2012a,b), which used a 4th order polynomial or 4 band ratio approach	Low at Stavely: compromised by other tranistion metal-bearing minerals (e.g. pyroxene). High in regolith and iron ore deposits (Rocklea case study: RMSE = 9.7%)
hem/goe (Hematite-goethite.txt)	Hematite/goethite ratio	Continuum removed wavelength of the 900 nm absorption minimum calculated using a fitted 12th order polynomial between 776 and 1150nm. 900W	R450 > R1650 + 900D >0.025	~900 nm: more hematitic	~940 nm: more goethitic	Haest et al. (2012a,b)	Moderate: wavelength accuracy of the iron-oxide crystal field absorption is adversely affected by mixing with green and dry vegetation as well as ferrous-bearing carbonate and silicate minerals
Kaolin abundance (Kaolin_abundance_2011v2.txt)	Kaolin group minerals: kaolinite halloysite, dickite and nacrite	2200D (Normalized depth of a fitted 4th order polynomial between 2120 and 2245 nm)	2160D [(R2138+R2190)/(R2156+R2179)] >1.005	0.04: low content	Not specified – depending on whole dataset	Sonntag et al. (2012)	High in regolith, low in low-metamorphic grade rocks: compromised by pyrophyllite and prehnite
Kaolin composition (Kaolin_comp_2011v2.txt)	Composition and crystallinity of kaolin group minerals ranging from well-ordered kaolinite to halloysite to dickite (and nacrite)	[(R2138+R2173)/R2156]/[(R2156+R2190)/R2173]	2200D>0.005	Not specified yet – depending on results from other drillcores	Not specified – depending on whole dataset	Sonntag et al. (2012)	Moderate, but compromised by pyrophyllite and prehnite
White mica abundance (wmAlsmai.txt)	Abundance of white micas (e.g. illite, muscovite, paragonite, brammalite, phengite, lepidolite, margarite) and smectites (montmorillonite, beidellite)	Relative absorption depth of the 2200 nm absorption for which the continuum is removed between 2120 and 2245, determined using a 3 band polynomial fit around the band with the lowest reflectance. 2200D3pfit	(R2326+R2376)/(R2343 + R2359) 2350DE >0.00035) + ((R2138+R2190)/(R2156 + R2179) 2160D2190 <1.063	0.04: low content	Not specified – depending on whole dataset	Further developed on the basis of Sonntag et al. (2012), which used a 4th order polynomial or 4 band ratio approach	Moderate: inherent errors related to the process of masking rather than umixing. That is, the threshold levels on mask parameters could exclude or include other materials especially for 'lower' levels. In sedimentary rocks at Stavely, problems with overlapping kaolinite
White mica composition (wmAlsmci.txt)	Tschermak substitution of white micas, ranging from paragonite, brammalite, to illite, muscovite to phengite, and smectites, ranging from beidellite to montmorillonite	Minimum wavelength of the 2200 nm absorption for which the continuum is removed between 2120 and 2245, determined using a 3 band polynomial fit around the band with the lowest reflectance. 2200W3pfit	(R2326+R2376)/(R2343 + R2359) 2350DE >0.00035) + ((R2138+R2190)/(R2156 + R2179) 2160D2190 <1.063	2185 nm: Al-rich mica (muscovite, illite, paragonite, brammalite, lepidolite)	2220 nm: Al-poor mica (~phengite)	Further developed on the basis of Sonntag et al. (2012), which used a 4th order polynomial or 4 band ratio approach	High: internationally established parameter for tracking Tschermak exchange in white micas and Al-smectites (e.g. Duke, 1994)
Chlorite–epidote abundance (chlepai3pfit.txt)	Chlorite, epidote, biotite	Relative absorption depth of the 2250 nm absorption for which the continuum is removed between 2230 and 2270, determined using a 3 band polynomial fit around the band with the lowest reflectance. 2250D3pfit	2250D3pfit >0.01, 2230 nm < 2250W < 2270 nm	0.04: low content	Not specified – depending on whole dataset	Further developed on the basis of Sonntag et al. (2012), which used a 4th order polynomial or 4 band ratio approach	Moderate: can be influenced by abundant jarosite, tourmaline, phlogopite. Probably some correlation with ferrous iron abundance
Chlorite–epidote composition (chlepci3pfit.txt)	Chlorite, epidote, biotite	Relative absorption depth of the 2250 nm absorption for which the continuum is removed between 2230 and 2270, determined using a 3 band polynomial fit around the band with the lowest reflectance. 2250D3pfit	2250D3pfit >0.01, 2230 nm < 2250W < 2270 nm	2248 nm: Mg-rich (Bishop et al., 2008)	2261 nm: Fe-rich (Bishop et al., 2008)	Further developed on the basis of Sonntag et al. (2012), which used a 4th order polynomial or 4 band ratio approach	Moderate: can be influenced by abundant jarosite, tourmaline, phlogopite. Probably some correlation with ferrous iron abundance
Carbonate abundance index TIR (6500P_3pfit.txt)	Calcite, dolomite, magnesite, siderite, ankerite	6500P Relative height of the reflectance peak between 6300 and 6700 nm, determined using a 3 band polynomial fit around the band with the highest reflectance		0.1	Not specified – depending on whole dataset	Inherited, unpublished	High, but lower threshold dependent on dataset
Carbonate composition index TIR1 (14000DW_3pfit.txt)	Calcite, dolomite, magnesite, siderite, ankerite	14000DW Minimum wavelength of the reflectance low between 13000 and 14000 nm, determined using a 3 band polynomial fit around the band with the lowest reflectance		13000 nm: Mg/Fe-rich	14000 nm: Ca-rich	Inherited, unpublished	High, but lower threshold dependent on dataset
Carbonate abundance (Carbonate_abundance_SWIR.txt)	Carbonates vs MgOH-bearing silicates, based on left-asymmetry of CO_3 feature @ 2340	Relative absorption depth of the 2340 nm absorption for which the continuum is removed between 2270 and 2370, determined using a 3 band polynomial fit around the band with the lowest reflectance. 2340D	2340D >0.04, 2295 nm < 2340W < 2360 nm, 2250D < 0.025, 2380D < 0.1117*2340D + 0.0002, Asymmetry of the 2340 absorption using a fitted 4th order polynomial between 2120 and 2370: 2340_left_asym > 1.13	0.05: low content	Not specified – depending on whole dataset	Further developed on the basis of Sonntag et al. (2012), which used a 4th order polynomial or 4 band ratio approach	Low: heavily impacted by grain size effects. False positives in case of mineral mixtures of, for example, white mica and chlorite
Carbonate composition SWIR (Carbonate_composition_SWIR.txt)	Separating calcite, dolomite, and siderite	Minimum wavelength of the 2340 nm absorption for which the continuum is removed between 2270 and 2370, determined using a 3 band polynomial fit around the band with the lowest reflectance. 2340W	2340D >0.04, 2295 nm < 2340W < 2360 nm, 2250D < 0.025, 2380D < 0.1117*2340D+0.0002, Asymmetry of the 2340 absorption using a fitted 4th order polynomial between 2120 and 2370: 2340_left_asym > 1.13	2303 nm: magnesite; 2326 nm: dolomite; recommendation for Stavely dataset: 2320 nm	2343 nm: calcite; recommendation for Stavely dataset: 2320 nm	Further developed on the basis of Sonntag et al. (2012), which used a 4th order polynomial or 4 band ratio approach	Moderate: works well for those carbonates, which are not masked out by the carbonate abundance index SWIR, The latter should be replaced by carbonate abundance index TIR
Amphibole–talc abundance (Amph_Talc_abundance.txt)	Abundance of amphibole and talc	2380D [(R2365+R2415)/(R2381+R2390)]	Composite mask* + MgOH abundance > 1.01 (+ 2160D2190 < 1.005)	1.005: low content	Not specified – depending on whole dataset	Laukamp et al. (2012)	Moderate: can be compromised by abundant phlogopite; noise
2080D3 (2080D3pfit.txt)	Depth of the 2080 feature, evident in talc. Useful for separating talc from amphiboles, the latter in general not showing this absorption feature	Depth of the 2080 nm absorption feature, for which the continuum is removed between 2060 and 2100, determined using a second order polynomial fitted through the 3 bands with the lowest reflectance. 2080D				Laukamp et al. (2012)	
2390W (2390W3pfit.txt)	Estimate of the Mg/Fe ratio (Mg#) in, for example, amphiboles and talc	Wavelength of absorption minimum calculated using a fitted fourth order polynomial between 2365 and 2430 nm, focused between 2380 and 2410 nm. 2390W		2382 nm: Mg-rich (Laukamp et al., 2012)	2406 nm: Fe-rich (Laukamp et al., 2012)	Laukamp et al. (2012)	
Quartz abundance	Quartz	8635D Relative depth of the 8626 nm Reststrahlen feature for which the continuum is removed between 8565 and 8705 nm, determined using a 3 band polynomial fit around the band with the lowest reflectance	no mask	0.1	Not specified – depending on whole dataset	Inherited, unpublished	High, but lower threshold dependent on dataset. Fractured drillcore can lead to extreme overestimation

References:

Bishop, JL, Lane, MD, Dyar, MD and Brown, AJ 2008, Reflectance and emission spectroscopy study of four groups of phyllosilicates: smectites, kaolinite-serpentines, chlorites and micas: Clay Minerals, v. 43, p. 35–54

Duke, E 1994, Near infrared spectra of muscovite, Tschermak substitution, and metamorphic reaction progress: Implications for remote sensing: Geology, v. 22, p. 621–624.

Haest, M, Cudahy, T, Laukamp, C and Gregory, S 2012a, Quantitative mineralogy from visible to shortwave infrared spectroscopic data. (I) Validation of mineral abundance and composition products of the Rocklea Dome channel iron deposit in Western Australia: Economic Geology, v. 107, p. 209–228.

Haest, M, Cudahy, T, Laukamp, C and Gregory, S 2012b, Quantitative mineralogy from visible to shortwave infrared spectroscopic data. (II) Three-dimensional mineralogical characterisation of the Rocklea Dome channel iron deposit, Western Australia: Economic Geology, v. 107, p. 229–249.

Laukamp, C, Termin, KA, Pejcic, B, Haest, M and Cudahy, T 2012, Vibrational spectroscopy of calcic amphiboles – applications for exploration and mining: European Journal of Mineralogy, v. 24, p. 863–878.

Sonntag, I, Laukamp, C and Hagemann, S 2012, Low potassium hydrothermal alteration in low sulfidation epithermal systems as detected by IRS and XRD: an example from the Co-O Mine, Eastern Mindanao, Philippines: Ore Geology Reviews, v. 45, p. 47–60.

RECORD 2016/19

MAPPING IRON ORE ALTERATION PATTERNS IN BANDED IRON-FORMATION USING HYPERSPECTRAL DATA: DRILLHOLE PK12DD001, MT RICHARDSON, YILGARN CRATON, WESTERN AUSTRALIA

Duuring and Laukamp

This Record is published in digital format (PDF) and is available as a free download from the DMP website at <www.dmp.wa.gov.au/GSWApublications>.

Further details of geological products produced by the Geological Survey of Western Australia can be obtained by contacting:

Information Centre
Department of Mines and Petroleum
100 Plain Street
EAST PERTH WESTERN AUSTRALIA 6004
Phone: +61 8 9222 3459 Fax: +61 8 9222 3444
www.dmp.wa.gov.au/GSWApublications